Chapter 2
Load Flow Calculation

The load flow is one of the most fundamental concepts in power system engineering. The basic function of the AVC system is to find out a feasible load flow in the grid, where the voltage profile of the whole system is within the acceptable operational band. This chapter will introduce the most popular and the newly proposed analytical method for the load flow calculations.

2.1 Load Flow Analysis

The objective of the load flow calculations is to obtain all node voltages and all branch currents. Generally, for a grid with n independent nodes, the following Eqs. (2.1)–(2.2) are valid.

$$\begin{bmatrix} Y_{11} & Y_{12} & \dots & Y_{13} \\ Y_{21} & Y_{22} & \dots & Y_{23} \\ \vdots & \vdots & \ddots & \vdots \\ Y_{n1} & Y_{n2} & \dots & Y_{nn} \end{bmatrix} \begin{bmatrix} v_1 \\ v_2 \\ \vdots \\ v_n \end{bmatrix} = \begin{bmatrix} i_1 \\ i_2 \\ \vdots \\ i_n \end{bmatrix} \tag{2.1}$$

$$[Y][v] = [i] \tag{2.2}$$

where $[v]$ is the node voltage vector and $[i]$ is the node current injection. Matrix $[Y]$ is the admittance matrix, where the diagonal element Y_{ii} is the self-admittance at node i that equals to the sum of all branch admittances connected to node i. The off-diagonal element of the admittance matrix Y_{ij} equals to the negative value of branch admittance connected between nodes i and j. If there is no branch between nodes i and j, then Y_{ij} equals to zero. For a normal transmission network, the admittance matrix is a sparse matrix, but not necessarily symmetrical due to the phase-shifting transformers. Figure 2.1 shows an example of an admittance matrix

© Springer International Publishing AG 2018

N. Qin, *Voltage Control in the Future Power Transmission Systems*,
Springer Theses, https://doi.org/10.1007/978-3-319-69886-1_2

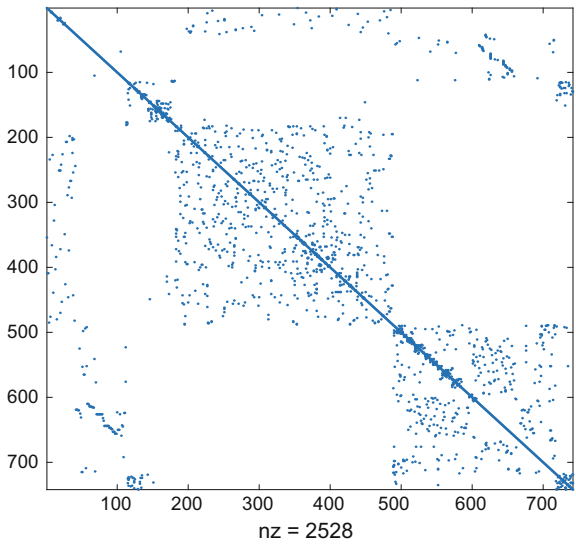


Fig. 2.1 The Danish transmission system admittance matrix

that represents the Danish transmission grid. It is highly sparse which requires fewer matrix factorizations than dense impedance matrix-based approaches, which is the reason for using the admittance matrix instead of the impedance matrix in load flow calculations.

Loads connected at nodes are included in branches. If all branch impedances are constant, including the constant impedance load, the load flow equations are linear, (2.3), where the constant impedance load is included in the system admittance matrix $[Y]$.

$$[Y][v] = 0 \tag{2.3}$$

However, the load at each node is typically modelled as constant power in the transmission grid, which turns the load flow equations to be nonlinear. The complex power is expressed as the product of the voltage and current vectors, which is represented in the polar form, (2.4). The current flow at each node is therefore represented in (2.5), where the current flowing into each node from other nodes equals to the current drawn by the complex power load at this node.

$$vi^* = VIe^{j(\delta_V - \delta_I)} = VIe^{j\emptyset} \tag{2.4}$$

$$\sum_{k=1}^{n} Y_{ik} v_k = \frac{P_i - jQ_i}{v_i^*},\ i \in \mathcal{V} \tag{2.5}$$

where P_i and Q_i are the total power injection at node i. They are found as (2.6)–(2.7).

$$P_i = P_{li} - P_{Gi} \tag{2.6}$$

$$Q_i = Q_{li} - Q_{Gi} \tag{2.7}$$

Equation (2.5) can be divided into real and imaginary parts. It results in two equations and four variables for each node, i.e. the node voltage magnitude V, the voltage angle δ, the node active power injection P and the node reactive power injection Q. Typically, to solve (2.5), two of them should be given at each node. According to the known variables, the nodes can be classified.

(i) PV node. The active power and the voltage magnitude at this type of node are known. This type of node usually represents the busbar where the voltage source is connected, e.g. generators equipped with excitation systems. The voltage angle and the reactive power are unknown. There are typically limits to constrain the reactive power variables, e.g. the generation capability curve constrains the generator reactive power output according to the active power production.

(ii) PQ node. The active power and the reactive power are known. This type of node usually represents the busbar where the load is connected, e.g. the power consumptions or the junction points of branches. However, the generator without voltage control abilities is also connected to PQ node, as a negative load to produce the current instead of consuming it. The PQ nodes are passive nodes, where the voltage magnitude and the voltage angle are the results of the current flow in the grid.

(iii) Slack (SL) node. It is also called reference node, as the voltage magnitude and the voltage angle are given. The voltage angles in other nodes are referred to the voltage angle at SL node. Since the system power loss is unknown, the active power and the reactive power at SL node are used to balance the system power. For each synchronous system, only one SL node can provide the reference voltage angle.

(iv) P and PVQ nodes. In practical applications, the voltage magnitudes at some nodes are remotely controlled by one or a group of generators [1]. As shown in Fig. 2.2, the node under control is typically a PQ node, e.g. a pilot node in

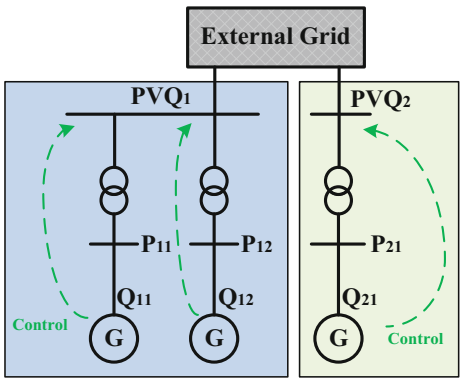


Fig. 2.2 Some nodes (at PVQ) are remotely controlled by one of a group of generators

Table 2.1 Summarized node type in the load flow calculation

Bus type		Data inputs	Unknown variables
SL		V, δ	P, Q
PQ		P, Q	V, δ
PV		P, V	δ, Q
Coupled	P	P, K	V, δ, Q
	PVQ	P, V, Q	δ

a voltage control system. In the case of a PQ node under remote control, this node becomes to a PVQ node, as the active power, the reactive power and the voltage magnitude are known. The controlling nodes connected by the dedicated generators, change from PV nodes to P nodes, as the generator reactive power are adjusted according to the needs at the corresponding PVQ nodes. The voltage magnitudes at P nodes are therefore unknown due to the reactive power regulations for maintaining the voltage at the PVQ node. In the case of several generators remotely controlling the voltage at a PVQ node, a participation factor of each generator is needed to share the reactive power outputs among them. The PVQ and P nodes are coupled, where the voltage magnitudes at PVQ nodes are maintained by the corresponding generators at P nodes.

Table 2.1 summarizes the node types in the load flow calculations, where K is the participation factor for the generators at P nodes to share the reactive power contribution for controlling the voltage at PVQ nodes. For a certain P/PVQ group, p, the individual generator output, Q_i complies with (2.8). It is valid for all N_p groups.

$$Q_i = K_i \sum_{i}^{N_{p,i}} Q_i \tag{2.8}$$

Since the voltage at SL node is already known, only $n-1$ node voltage magnitudes and voltage angles need to be calculated. The total number of load flow equations is $2(n-1)$. The power injection at SL node is found when all voltages are obtained.

2.2 Newton-Raphson Method

The most popular approach to solve the load flow equations is Newton-Raphson (NR) method [2]. The principle is to linearize the load flow equations by expanding the load flow equations with the Taylor series and neglecting the second and higher order terms. The compact form of the load flow equation can be expressed in (2.9), where x is unknown variables. The objective of (2.9) is to find out x, with which (2.9) can be valid, i.e. the system power is balanced for all nodes.

Applying the NR method to solve it, an initial guess for the unknown variables, x^0, is needed. The difference between the initial guess and the final solution is thus

Δx^0. Equation (2.10) is obtained, by replacing the final solution x with the initial guess, x^0, and the differences, Δx^0. Therefore, if Δx^0 is known, then x can be obtained and the problem is solved. In order to derive the differences, Δx^0. Equation (2.10) is expanded with Taylor series, shown in (2.11).

$$g(x) = 0 \tag{2.9}$$

$$g\left(x^0 + \Delta x^0\right) = 0 \tag{2.10}$$

$$g\left(x^0 + \Delta x^0\right) = g\left(x^0\right) + g_x\left(x^0\right)\Delta x^0 + \cdots + g_x^n\left(x^0\right)\frac{\left(\Delta x^0\right)^n}{n!} = 0 \tag{2.11}$$

If neglecting the second and higher order terms in (2.11), a linear equation is obtained in (2.12).

$$g\left(x^0\right) + g_x\left(x^0\right)\Delta x^0 = 0 \tag{2.12}$$

$$\Delta x^0 = -\frac{g(x^0)}{g_x(x^0)} \tag{2.13}$$

where g_x is the first order derivative of the load flow function $g(x)$ w.r.t. x, which is also called Jacobian matrix where typically more than one unknown variables are presented in g_x. The differences, Δx^0, is then obtained via (2.13). The new values of the unknown variables, x, can thus be obtained as shown in (2.14).

$$x^1 = x^0 + \Delta x^0 = x^0 - \frac{g(x^0)}{g_x(x^0)} \tag{2.14}$$

Substituting x^1 to (2.9) for evaluating the result, if (2.9) is not valid, then x^1 is the new guess and a new iteration is needed to carried out. A general iteration step is presented in (2.15). The iteration will stop if (2.16) is fulfilled, i.e. the maximum power mismatch at the nodes in the load flow equation, $\left\|g\left(x^k\right)_n\right\|$, is less than the predefined convergence precision, ε, that is a small positive number.

$$x^{k+1} = x^k + \Delta x^{k+1} = x^k - \frac{g\left(x^k\right)}{g_x\left(x^k\right)} \tag{2.15}$$

$$\left\|g\left(x^k\right)\right\|_n < \varepsilon \tag{2.16}$$

2.2.1 Load Flow with Newton-Raphson Method

Applying NR method to solve the load flow equations, the node voltages and branch admittances can be expressed in the polar form, (2.17)–(2.18).

$$V_i \sum_{k=1}^{N_v} V_k (G_{ik} \cos \delta_{ik} + B_{ik} \sin \delta_{ik}) = P_i, \quad \forall i \in \mathcal{V} - \{ref\} \tag{2.17}$$

$$V_i \sum_{k=1}^{N_v} V_k (G_{ik} \sin \delta_{ik} - B_{ik} \cos \delta_{ik}) = Q_i, \quad \forall i \in \mathcal{V} - \{ref\} \tag{2.18}$$

If the left-hand-side of (2.17) and (2.18) are defined as $P(x)$ and $Q(x)$, respectively, then the load flow equations are expressed in (2.19).

$$g\left(x^k\right) = \begin{bmatrix} P\left(x^k\right) - P_i \\ Q\left(x^k\right) - Q_i \end{bmatrix} = \begin{bmatrix} \Delta P^k \\ \Delta Q^k \end{bmatrix}, \quad k = 0, 1, 2 \ldots \tag{2.19}$$

where the right-hand-side of (2.19) is the power mismatches at node i in the iteration k. In the polar form, only the voltage magnitudes, V, and the voltage angles, δ, need to be determined via the NR method. The unknown reactive power injections at PV and P nodes, and the active power and the reactive power injections at SL nodes are calculated through (2.17)–(2.18) afterwards. Substituting (2.19)–(2.15), yields (2.20).

$$\begin{bmatrix} \Delta P^k \\ \Delta Q^k \end{bmatrix} = -J \begin{bmatrix} \Delta \delta^{k+1} \\ \Delta V^{k+1} \end{bmatrix}, \quad k = 0, 1, 2 \ldots \tag{2.20}$$

$$\Delta P = [\Delta P_{PV} \quad \Delta P_{PQ} \quad \Delta P_P \quad \Delta P_{PVQ}]^\intercal \tag{2.21}$$

$$\Delta Q = \left[\Delta Q_{PQ} \quad [\Delta Q_{PVQ} \quad \Delta Q_{P(n_P - n_{PVQ})}]^\intercal\right]^\intercal \tag{2.22}$$

$$\Delta x = [\Delta \delta_{PV} \quad \Delta \delta_{PQ} \quad \Delta \delta_P \quad \Delta \delta_{PVQ} \quad \Delta V_{PQ} \quad \Delta V_P]^\intercal \tag{2.23}$$

where J is the Jacobian matrix representing the first-order derivatives of the powr mismatches w.r.t. the voltage angles and the voltage magnitudes, respectively. The color marked in (2.21)–(2.23) indicates that the lengths of the vectors are the same marked with the same color. According to Table 2.1, in the polar form, the active power mismatches are found for PQ, PV, P and PVQ nodes, and the reactive power mismatches are found for PQ and PVQ nodes at iterations. Moreover, the reactive power mismatches at PVQ nodes are mainly removed by regulating the voltage at the corresponding P nodes. Therefore, if defining the power mismatches as (2.21)–(2.22) according to Table 2.1 and unknown variables as (2.23), then the Jacobian matrix is expressed in (2.24).

Note that if a PVQ node is remotely controlled by several P nodes, then only one of the P nodes will be used to accommodate the reactive power mismatch caused by controlling the voltage at PVQ node in (2.22), i.e. ΔQ_{PVQ} is corresponding to only one ΔV_P, though there may be several P nodes in this PVQ/P pair. It is used to

maintain the full rank of the Jacobian matrix. The length of $[\Delta Q_{PVQ}\ \Delta Q_{P(n_P-n_{PVQ})}]^{\mathrm{T}}$ equals to the number of P nodes, n_P. The reactive power injections for the other P nodes are dispatched according to the contribution factors through (2.8) at iterations.

$$J = \begin{bmatrix} J_1 & J_2 \\ J_3 & J_4 \end{bmatrix} \tag{2.24}$$

If defining the numbers of nodes as n_{PV}, n_{PQ}, n_P and n_{PVQ}, and the total number of nodes is n, then:

J_1 is a $(n-1) \times (n-1)$ matrix, where the entries are $\frac{\partial P}{\partial \delta}$.
J_2 is a $(n-1) \times (n_{PQ}+n_P)$ matrix, where the entries are $\frac{\partial P}{\partial V}$.
J_3 is a $(n_{PQ}+n_P) \times (n-1)$ matrix, where the entries are $\frac{\partial Q}{\partial \delta}$.
J_4 is a $(n_{PQ}+n_P) \times (n_{PQ}+n_P)$ matrix, where the entries are $\frac{\partial Q}{\partial V}$.

The expressions of the entries in Jacobian matrix are presented in Appendix B—Derivative.

The algorithm for solving the load flow equations is shown in Table 2.2, where the inputs to the algorithm are the system admittance matrix, the initial guess of the unknown variables and the known data for different types of nodes according to Table 2.1. In case P/PVQ nodes are absent from the systems, then only ΔP for PV and PQ nodes and ΔQ for PQ nodes are used to find out the corresponding incremental variables $\Delta\delta$ and ΔV. The corresponding Jacobian matrices J_1, J_2, J_3 and J_4, are then modified to exclude the P and PVQ nodes. Line 8 in Table 2.2 is removed, accordingly.

Note that even though the reactive power injections and the voltage magnitudes at PVQ nodes are known, the attendance of reactive power mismatch at PVQ nodes

Table 2.2 The load flow algorithm applying Newton-Raphson method

1	*Calculate ΔP for PV, PQ, PVQ and P nodes, and ΔQ for PQ, PVQ and P nodes, (2.19);*
2	*if $\|\Delta P\|_n \geq \varepsilon$ or $\|\Delta Q\|_n \geq \varepsilon$*
3	*while $i_{tr} \leq N_{max}$*
4	*Calculate Jacobian matrix, (2.24);*
5	*Calculate $\Delta\delta$ for PV, PQ, PVQ and P nodes, and ΔV for PQ and P nodes;*
6	*Update δ and V, (2.15);*
7	*Calculate power flow in the branches through (2.17)-(2.18);*
8	*Accommodate the reactive power output for each P node with participation factor K, (2.8);*
9	*Calculate ΔP for PV, PQ, PVQ and P nodes, and ΔQ for PQ, PVQ and P nodes, (2.19);*
10	*if $\|\Delta P\|_n < \varepsilon$ and $\|\Delta Q\|_n < \varepsilon$*
11	*break;*
12	*end*
13	*end*
14	*end*

in (2.22) is to provide the relation between the reactive power mismatches at PVQ nodes and the voltage magnitudes at corresponding P nodes. In other words, PVQ and P nodes comply with two relations that should be addressed in the algorithms: (i) Maintaining the voltage magnitude at PVQ nodes results in reactive power mismatch at PVQ nodes that should be removed by adjusting the voltage magnitudes at corresponding P nodes. (ii) The share of the reactive power injections at P nodes comply with (2.8).

An example is demonstrated by applying the algorithm in Table 2.2, where the IEEE-39 bus system is used with modifications. Two P/PVQ pairs are defined as marked in Fig. 2.3, i.e. Gen 31 and Gen 32 remotely control the voltage magnitude at Bus 11, and Gen 35 and Gen 36 remotely control the voltage magnitude at Bus 22, presented in Table 2.3. Generator Gen 30, Gen 33, Gen 34, Gen 37 and Gen 38 are connected to PV nodes which control their terminal voltage magnitudes. Gen 39 is the slack machine. For the PV and PVQ nodes, the initial voltage magnitudes are set as target values.

The calculation is converged after 6 iterations, where the maximum power mismatch is smaller than $1e-8$ pu. In contrast, if the reactive power mismatch at PVQ nodes in (2.22) is absent, the calculation will also be converged after 18

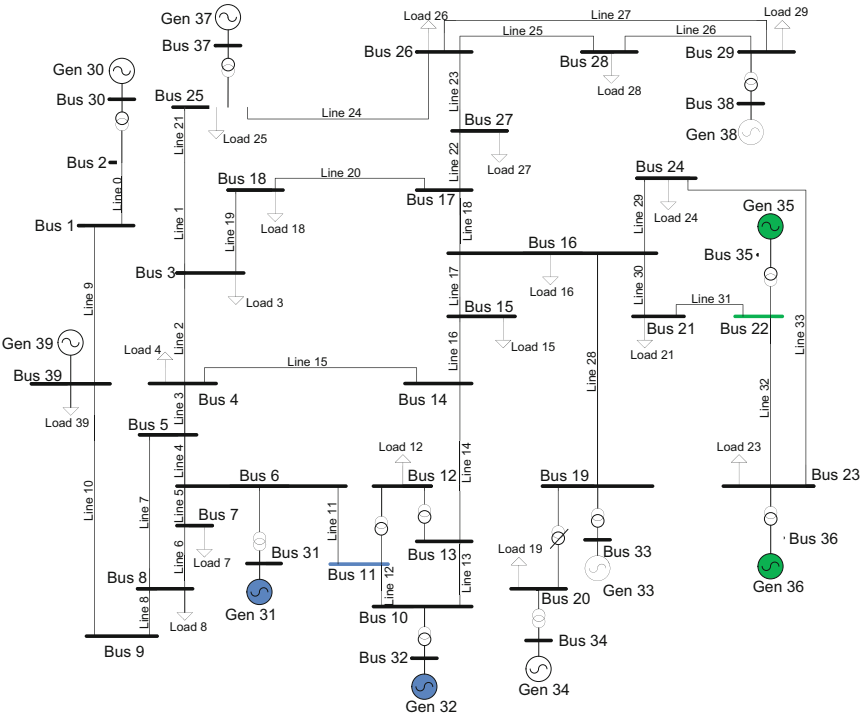


Fig. 2.3 IEEE-39 bus system, where Gen 31 and Gen 32 remotely control Bus 11 voltage in blue, and Gen 35 and Gen 36 remotely control Bus 22 voltage in green

Table 2.3 Defined PVQ/P pairs in the test grid shown in Fig. 2.3

P nodes	PVQ nodes	V at PVQ nodes (pu)	K for P nodes
31	11	1.03	0.468
32			0.532
35	22	1.02	0.537
36			0.463

iterations. Some of the node results from two study cases are summarized in Table 2.4. In both cases, the voltage magnitudes at PVQ nodes are maintained as target values. However, reactive power injections at corresponding P nodes are different. From Table 2.4, it can be seen that the share of the reactive power contributions for P nodes at each P/PVQ pair are the same for both cases, but the total reactive power injections at each P/PVQ pair are different due to missing sensitivities of reactive power change at PVQ node w.r.t. the corresponding voltage magnitudes at P nodes in each P/PVQ pair. In fact, without taking power mismatches at PVQ nodes in (2.22), the corresponding voltage magnitudes at P nodes will also be absent. These P nodes are therefore treated as PV nodes, i.e. the voltage magnitudes are known and then do not participate in iterations. The rest of P nodes are still presented in the iterations, treated as PQ nodes. There is only one more constraint, i.e. the share of reactive power injections among the P nodes in the same PVQ/P pair should correspond to the contribution factor. Therefore, the reactive power dispatch among P nodes is carried out at iterations for which the terminal voltages at the presented P nodes are adjusted in order to comply with the contribution factors of the reactive power injections. In Table 2.4, though the result in Case (ii) without ΔQ_{PVQ} terms in (2.22) also seems reasonable; however, it needs more iterations than Case (i) due to missing the derivation of $\frac{\Delta Q_{PVQ}}{\Delta V_P}$. These cases also

Table 2.4 Results comparison

Case		(i) with ΔQ_{PVQ}				(ii) without ΔQ_{PVQ}			
Iterations		6				18			
Nodes		V (pu)	δ (deg)	P (MW)	Q (MVar)	V (pu)	δ (deg)	P (MW)	Q (MVar)
Type	Index								
PVQ	11	***1.030***	3.898	–	–	***1.030***	3.933	–	–
PVQ	22	*1.020*	10.933	–	–	*1.020*	10.953	–	–
P	31	1.087	9.801	572.93	***294.62***	***1.030***	10.375	572.93	***100.60***
P	32	1.024	12.219	650.00	***334.91***	0.974	12.756	650.00	***114.36***
P	35	1.017	16.201	650.00	*187.90*	*1.020*	16.207	650.00	*207.28*
P	36	1.053	18.830	560.00	*162.00*	1.058	18.796	560.00	*178.71*
PQ	1	1.041	1.559	–	–	1.040	1.564	–	–
PV	33	0.997	13.643	632.00	187.88	0.997	13.669	632.00	192.55
SL	39	1.030	0	108.18	158.20	1.030	0	108.84	137.99

(i) with ΔQ_{PVQ} in (2.22); (ii) without ΔQ_{PVQ} in (2.22); Two P/PVQ pairs marked with blue and green respectively, according to Fig. 2.3

demonstrate that multiple solutions exist for the load flow equations complying with generator remote voltage control constraints.

In summary, NR method can be applied to solve the load flow equations. It is a tangent-based search method that iteratively calculates the adjustment quantities at unknown variables based on the known mismatch values at nodes. The slack nodes are used to absorb the power mismatches to keep the validity of the power balance equations. This method requires initial guesses for unknown variables that should be sufficiently close to the target points. Some control functions can be embedded into the load flow equations, such as generator local/remote voltage control, and the transformer tap changes and the shunt couplings for the voltage control in the load flow calculations.

The main challenge of NR method is to provide a "good" initial guess sufficiently close to the target, which in many cases, especially in abnormal situations, is very difficult. It means that some physically existing solutions are incapable of being found via classical NR method if the initial guesses are "far away" from the target values. In addition, the exact convergence boundary is not able to be identified.

A variety of robust improvements of the basic NR method have been proposed in the literature for solving ill-conditioned cases [3–5]. The widely used method is optimal multiplier method, which adjusts the step-size of the updated unknown variables to improve the convergence properties of the iterative process. For the unsolvable cases where no solution exists, either the continuation power flow techniques can be applied to track on the maximum loadability [6], or Holomorphic embedding load flow method (HELM) can be applied for identifications [7].

2.3 Holomorphic Embedding Load Flow Method

HELM is proposed by Antonio Trias, which is a breakthrough approach to solve the load flow equations [7]. In contrast to NR method, HELM provides an analytical solution in a recursive manner, which is independent of initial guesses. It guarantees to provide the stable equilibrium point of the load flow problem if it physically exists [7–11]. The load flow calculation with pure PQ nodes and a slack node is presented in [7]. Furthermore, the model including PV nodes is more complex, which is presented in [8–11]. However, HELM is still not popular in the power system engineering society, as there are only a few papers to present the detailed implementations that can be used for inspiring other researches for applications.

2.3.1 The HELM Concept

A holomorphic function is a complex-valued function of one or several complex variables. It is complex differentiable in the neighborhood of every point in the

complex domain. The holomorphic function is also an analytical function that can be represented by a converged power series where the coefficients are complex values [7], (2.25).

$$f(z) = \sum_{n=0}^{\infty} C_n (z - z_0)^n \tag{2.25}$$

The idea of HELM is to embed the load flow equations into a large solution space by casting the voltage variables to complex-valued power series in which the analytical solution is trivial to find under a certain condition, e.g. no load condition [9]. This solution is a so-called germ solution, (2.26), that is an analytical solution of the power series (2.25) under a specified condition, where z_0 is the constant complex value, and $C_1, C_2, \ldots$ are the complex power series coefficients for different orders.

$$g = (z_0, C_1, C_2, \ldots) \tag{2.26}$$

The solution of the original load flow equations represented by power series is then obtained based on this germ solution through the analytical continuation techniques, i.e. Padé approximants [12].

The concept can be demonstrated in Fig. 2.4. After embedding the load flow equations to the s-plane, the load flow equations are analytical and can be casted to power series. In Fig. 2.4, a quadratic function is used to demonstrate the analytical function. For the embedded load flow equations, it is generally a Taylor series with several orders. The coefficients of the power series in the load flow equations are trivial to be found under a certain condition, e.g. $s = 0 + j0$. The coefficients under $s = 0 + j0$ is thus a germ solution of the load flow equation w.r.t s. In order to

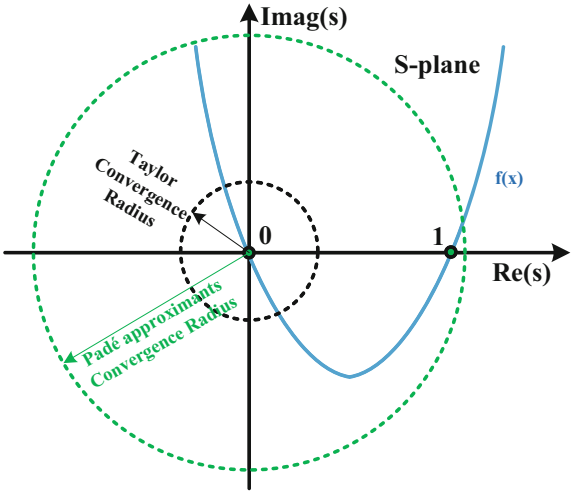


Fig. 2.4 The sketch of HELM concept

obtain the solution to the original load flow equation, e.g. $s = 1$ should be substituted. However, the convergence radius of Taylor series may not sufficiently cover the solution space where $s = 1$. Therefore, analytical continuation technique is applied to extend the convergence radius to be the largest value [7]. In addition, if the embedded load flow can be converged with the analytical continuation, then there is a physical solution. Otherwise, there is no solution [7].

Comparing to the continuation load flow method that uses the numerical prediction-correction step to track the "nose" curve, HELM is not able to be converged at the maximum loadability point. The numerical continuation method adds a new dimension to overcome the singularity of the Jacobian matrix at the breaking point whereas HELM applies the analytical continuation techniques that fail to be converged at the breaking point. In other words, the continuation load flow method is able to exhibit the entire "nose" curve by increasing the embedded scalar, whereas HELM theoretically needs at least two germ solutions for drawing the upper and lower branches of "nose" curve separately.

2.3.2 *Padé Approximantion*

Padé approximants are rational approximants to the power series, whose convergence has been known to be much better than that of power series. The largest radius of convergence for these power series can be obtained through Padé approximants, as stated by Stahl's Padé convergence theory [13–14]. The Padé approximation method is briefly introduced in the following statements.

A Taylor series with $M+N$ orders is able to be approximated by rearranging into a ratio of two such expansions with M orders in nominator and N orders in the denominator, (2.27), where a_n and b_n are coefficients, respectively. The denominator is normalized that $b_0 = 1$.

$$C_0 + C_1 x + C_2 x^2 + \cdots = \frac{a_0 + a_1 x + a_2 x^2 + \cdots}{1 + b_1 x + b_2 x^2 + \cdots} = \frac{\sum_{n=0}^{N} a_n x^n}{\sum_{n=0}^{M} b_n x^n} \tag{2.27}$$

Moving the denominator to the left-hand-side and equating the coefficients of each order, yields (2.28).

$$\begin{array}{rcl} \boldsymbol{a_0} & = & \boldsymbol{C_0} \\ \boldsymbol{a_1} & = & \boldsymbol{C_1} + C_0 b_1 \\ \boldsymbol{a_2} & = & \boldsymbol{C_2} + C_1 b_1 + C_0 b_2 \\ \vdots & \vdots & \vdots \\ \boldsymbol{a_N} & = & \boldsymbol{C_N} + C_{N-1} b_1 + \cdots + C_0 b_N \\ \hline \boldsymbol{0} & = & \boldsymbol{C_{N+1}} + C_N b_1 + \cdots + C_{N-M+1} b_M \\ \vdots & \vdots & \vdots \\ \boldsymbol{0} & = & \boldsymbol{C_{N+M}} + C_{N+M-1} b_1 + \cdots + C_N b_M \end{array} \tag{2.28}$$

As shown in (2.28), there is total $(M+N)$ orders for C-series, $\{C_n x^n\}$ but only N orders for $\{a_n x^n\}$. Therefore, the coefficients of $\{b_n x^n\}$ can be obtained by solving M equations in the bottom of (2.28), marked with green color, which is formulated in (2.29). The coefficients of $\{a_n x^n\}$ are thus obtained by solving the fist N equations afterwards, (2.30). This is also called Direct Method of Padé approximation [10].

$$\begin{bmatrix} C_{N-M+1} & C_{N-M+2} & C_{N-M+3} & \cdots & C_N \\ C_{N-M+2} & C_{N-M+3} & C_{N-M+4} & \cdots & C_{N+1} \\ C_{N-M+3} & C_{N-M+4} & C_{N-M+5} & \cdots & C_{N+2} \\ \vdots & \vdots & \vdots & \ddots & \vdots \\ C_N & C_{N+1} & C_{N+2} & \cdots & C_{N+M-1} \end{bmatrix} \begin{bmatrix} b_M \\ b_{M-1} \\ b_{M-2} \\ \vdots \\ b_1 \end{bmatrix} = - \begin{bmatrix} C_{N+1} \\ C_{N+2} \\ C_{N+3} \\ \vdots \\ C_{N+M} \end{bmatrix} \tag{2.29}$$

$$\sum_{k=0}^{n} C_k b_{n-k} = a_n, \quad n = 1, 2 \ldots N \tag{2.30}$$

The results of Padé approximation create a $M \times N$ matrix with entries representing quotients of two power series, r representing $\{a\}$ and $\{b\}$ at a certain order of x. The matrix is called Padé table [16], shown in (2.31). If $M = 0$, then only the first row is remained, which is the original power series.

$$\begin{matrix} r_{0,0} & r_{0,1} & r_{0,2} & r_{0,3} & \cdots \\ r_{1,0} & r_{1,1} & r_{1,2} & r_{1,3} & \cdots \\ r_{2,0} & r_{2,1} & r_{2,2} & r_{2,3} & \cdots \\ r_{3,0} & r_{3,1} & r_{3,2} & r_{3,3} & \cdots \\ \vdots & \vdots & \vdots & \vdots & \ddots \end{matrix} \tag{2.31}$$

2.3.3 Continued Fraction

As stated in Stahl's Padé convergence theory [13, 14], the diagonal and paradiagonal Padé approximants provide the maximal analytic continuation. The diagonal and paradiagonal Padé approximants coincide with the continued fraction approximation to the power series. The continued fraction is connected to Padé approximants according to the theory [15].

"*Let $f(x)$ be a given Finite Taylor Series. If every three consecutive elements in the descending staircase of Padé approximants sequence are distinct, then there exists a regular continued fraction corresponding to $f(x)$*".

In the theory stated in [16], the partial numerators of the regular continued fraction correspond to the coefficients of the Taylor series, (2.32), where K_m^{∞} stands for the continued fraction operation.

$$f(x) = C_0 + \cfrac{\bar{C}_{10}x}{1 + \cfrac{\bar{C}_{20}x}{1 + \cfrac{\bar{C}_{30}x}{1 + \cfrac{\bar{C}_{m0}x}{1 + \cdots}}}} = K_{m=1}^{\infty}\left(\frac{\bar{C}_{m0}}{1}\right), \quad \bar{C}_{m0} \neq 0 \tag{2.32}$$

In order to connect the Taylor power series, the Viskovatov method can be applied [16]. Considering a Taylor series $\{C_n x^n\}$, if two series are defined, $\bar{C}_{0j}$ and $\bar{C}_{1j}$ complying with (2.33)–(2.34), then (2.35) can be derived [16]. Once $\bar{C}_{m,0}, m = 1, 2\ldots$ is found, $f(x)$ can be evaluated through (2.32).

$$\bar{C}_{0j} = \begin{cases} 1, & j = 0 \\ 0, & j > 0 \end{cases} \tag{2.33}$$

$$\bar{C}_{1j} = C_{j+1}x^{j+1}, \quad j \geq 0 \tag{2.34}$$

$$\bar{C}_{m,j} = \frac{\bar{C}_{m-2,j+1}}{\bar{C}_{m-2,0}} - \frac{\bar{C}_{m-1,j+1}}{\bar{C}_{m-1,0}}, \quad m \geq 2, \quad j \geq 0 \tag{2.35}$$

In the load flow calculation, a matrix for each node voltage is created, as shown in (2.36), and filled by the two power series, $\{\bar{C}_{0j}\}$ and $\{\bar{C}_{1j}\}$ shown in (2.33)–(2.34), into the first two rows. The goal is to find out $\bar{C}_{m,0}$ as many as possible according to the original Taylor series coefficients, i.e. expanding the matrix (2.36) as much as possible until convergence if there is a solution to the original problem.

$$\begin{array}{cccccc} \mathbf{1} & \mathbf{0} & \mathbf{0} & \mathbf{0} & \mathbf{0} & \cdots \\ \boldsymbol{C_1} & \boldsymbol{C_2} & \boldsymbol{C_3} & \boldsymbol{C_4} & \boldsymbol{C_5} & \cdots \\ \bar{C}_{2,0} & \bar{C}_{2,1} & \bar{C}_{2,2} & \bar{C}_{2,3} & \bar{C}_{2,4} & \cdots \\ \bar{C}_{3,0} & \bar{C}_{3,1} & \bar{C}_{3,2} & \bar{C}_{3,3} & \bar{C}_{3,4} & \cdots \\ \bar{C}_{4,0} & \bar{C}_{4,1} & \bar{C}_{4,2} & \bar{C}_{4,3} & \bar{C}_{4,4} & \cdots \\ \vdots & \vdots & \vdots & \vdots & \vdots & \ddots \end{array} \tag{2.36}$$

Pick up the **first column** to construct the continued fraction $K_{m=1}^{\infty}\left(\frac{\bar{C}_{m0}}{1}\right)$. The value of $f(x)$ can be obtained hereafter by adding the constant value C_0 through (2.32).

Alternatively, the value of the continued fraction can be found through a three-term recursive relationship which is equivalent to either a diagonal or para-diagonal Padé approximant, marked in red in (2.31). The recursive relations of the continued fraction, (2.32), can be expressed in (2.37) [16].

$$\begin{bmatrix} A_m \\ B_m \end{bmatrix} := \begin{bmatrix} A_{m-1} \\ B_{m-1} \end{bmatrix} + \bar{C}_{m0}\begin{bmatrix} A_{m-2} \\ A_{m-2} \end{bmatrix}, \quad \bar{C}_{m0} \neq 0 \; for \; m \geq 1 \tag{2.37}$$

where $A_{-1} := 1, \quad B_{-1} := 0, \quad A_0 := C_0 \; and \; B_0 := 1$ are initial values. Equation (2.37) is finally applied to evaluate the Padé approximation for the load flow calculations.

2.3.4 Load Flow Solution with HELM

As mentioned above, the idea to solve the load flow equations with HELM is to place the load flow equations into a large solution space through embedding. After embedding a complex variable, the load flow equations are infinitely differentiable w.r.t. this complex variable which is analytical, also called holomorphic in the complex analysis.

The power flow equations shown in (2.5) are embedded with a complex variable s, where the voltage is considered as a function of the embedded variable s, as shown in (2.38). It can be seen that if $s = 0$, (2.38) is converted to (2.3) which is trivial to be solved. If $s = 1$, then (2.38) represents the original load flow equations without the embedding.

$$\sum_{k=1}^{n} Y_{ik} v_k(s) = \frac{(P_i - jQ_i)s}{v_i^*(s^*)} \tag{2.38}$$

The holomorphicity guarantees that the voltage can be represented as an equivalent power series of the embedding complex variable s, (2.39) [9], where $v_i[n]$ represents a complex coefficient at order n of the power series w.r.t. s at the node i.

$$v_i(s) = \sum_{n=0}^{\infty} v_i[n] s^n \tag{2.39}$$

Note that the conjugate voltage in (2.38) is embedded as $v_i^*(s^*)$ in order to maintain holomorphicity, as shown in (2.40) [11] where the conjugated voltage is also a function of the embedded s.

$$v_i^*(s^*) = v_i[0]^* + v_i[1]^* s + v_i[2]^* s^2 + \cdots + v_i[n]^* s^n \tag{2.40}$$

Equation (2.38) is generally valid for all nodes in the system. In the case of PV node, the voltage magnitude is constant and the reactive power injection is unknown. It means that there is one more unknown variable, Q_i, and one more voltage magnitude constraint than (2.38) at each PV node. The unknown reactive power can be embedded, as $Q_i(s)$, for the PV node i [9]. Similarly, for the PVQ nodes, not only the active power and the reactive power, but also the voltage magnitude is known.

Equations (2.41)–(2.47) can be obtained, which is the so-called canonical embedding [9]. Other embedding methods are also valid as shown in [8, 11]. The Eqs. (2.44)–(2.45) for PVQ nodes are the same with (2.41) and (2.43) for the PQ and PV nodes, respectively. The voltage magnitudes and the reactive power injections at the corresponding P nodes are unknown where (2.46) is similar to (2.42), but the unknown reactive power injections complies with the contribution factors among the P nodes in the same P/PVQ pair. Note that the embedded variable s in the unknown reactive power variable, $Q_i(s)$ in (2.42) and (2.46), is a real

variable. This condition indicates that the analytical path from $s = 0$ to $s = 1$ is along the real axis, though s itself is a complex variable. It is a valid assumption as the calculations will not trace the whole path, only two points need to be solved, i.e. $s = 0$ for the no load condition as a germ solution, and $s = 1$ for the original load flow equations.

Type	Load flow equations with embedding variable s	
PQ	$\sum_k Y_k^{tr} v_k(s) = s\frac{P_{PQ} - jQ_{PQ}}{v_{PQ}^*(s)} - sY^{sh} v_{PQ}(s)$	(2.41)
PV	$\sum_k Y_k^{tr} v_k(s) = \frac{sP_{PV} - jQ_{PV}(s)}{v_{PV}^*(s)} - sY^{sh} v_{PV}(s)$	(2.42)
	$v_{PV}(s) v_{PV}^*(s) = 1 + s\left(V_{PV}^{sp^2} - 1\right)$	(2.43)
PVQ	$\sum_k Y_k^{tr} v_k(s) = s\frac{P_{PVQ} - jQ_{PVQ}}{v_{PVQ}^*(s^*)} - sY^{sh} v_{PVQ}(s)$	(2.44)
	$v_{PVQ}(s) v_{PVQ}^*(s^*) = 1 + s\left(V_{PVQ}^{sp^2} - 1\right)$	(2.45)
P	$\sum_k Y_k^{tr} v_k(s) = \frac{sP_P - jK_i \sum Q_P(s)}{v_P^*(s^*)} - sY^{sh} v_P(s)$	(2.46)
SL	$v_{slack}(s) = 1 + s\left(V_{SL}^{sp^2} - 1\right)$	(2.47)

If casting all embedded variables of (2.41)–(2.47) to the power series by defining (2.39) and (2.48)–(2.50) for the unknown voltages and the reactive power injections, the Eqs. (2.51)–(2.55) can be obtained. These equations are closed to determine the load flow solution analytically, where V_i^{sp} is the known voltage magnitude at node i for PVQ and PV nodes. Y_i^{sh} is the shunt admittance at node i. Y_{ik}^{tr} is the series admittance between node i and k.

$$Q_i(s) = \sum_{n=0}^{\infty} Q_i[n] s^n \tag{2.48}$$

$$\frac{1}{v_i(s)} = w_i(s) = \sum_{n=0}^{\infty} w_i[n] s^n \tag{2.49}$$

$$\frac{1}{v_i^*(s^*)} = w_i^*(s^*) = \sum_{n=0}^{\infty} w_i^*[n] s^n \tag{2.50}$$

$$\sum_k Y_{ik}^{tr} \sum_{n=0}^{\infty} v_k[n] s^n = (P_i - jQ_i) \sum_{n=0}^{\infty} w_i^*[n] s^{n+1} - Y_i^{sh} \sum_{n=0}^{\infty} v_i[n] s^{n+1} \tag{2.51}$$

$$\sum_k Y_{ik}^{tr} \sum_{n=0}^{\infty} v_k[n] s^n = \left(sP_i - j \sum_{n=0}^{\infty} Q_i[n] s^n\right) \sum_{n=0}^{\infty} w_i^*[n] s^n - Y_i^{sh} \sum_{n=0}^{\infty} v_i[n] s^{n+1} \tag{2.52}$$

$$\sum_{n=0}^{\infty} v_i[n]s^n \sum_{n=0}^{\infty} v_i^*[n]s^n = 1 + s\left(V_i^{sp^2} - 1\right) \tag{2.53}$$

$$\sum_{k} Y_{ik}^{tr} \sum_{n=0}^{\infty} v_k[n]s^n = \left(sP_i - j\sum_{n=0}^{\infty} K_i Q_\Sigma[n]s^n\right) \sum_{n=0}^{\infty} w_i^*[n]s^n - Y_i^{sh} \sum_{n=0}^{\infty} v_i[n]s^{n+1} \tag{2.54}$$

$$\sum_{n=0}^{\infty} v_i[n]s^n \sum_{n=0}^{\infty} w_i[n]s^n = 1 \tag{2.55}$$

As shown in Table 2.5, for PQ nodes, there are 2 unknown power series, i.e. $v_i(s)$ and $w^* = \frac{1}{v_i^*(s^*)}$, and 2 sets of corresponding equations, (2.51) and (2.55) for power flow and the reciprocal relation of the 2 unknown power series. For PV nodes, there are 1 more unknown power series than PQ nodes, $Q_i(s)$, and total 3 sets of corresponding equations, (2.52)–(2.53) and (2.55), where (2.53) is used to constrain the voltage magnitude.

For PVQ nodes, the number of unknown power series are the same with that for the PQ nodes, but 1 more set of corresponding equation than PQ nodes, (2.53), for the voltage magnitude constraints. For the P nodes, there are 3 unknown power series, but only 2 sets of corresponding equations are valid. However, P and PVQ nodes are always coupled. Therefore, the redundant sets of equations for PVQ nodes need to compensate the missing sets of equations for P nodes. The total numbers of unknown power series and the corresponding equations are equal. The problem can thus be solved.

In each equation of (2.52)–(2.55), there is a multiplication of two power series. A common convolution formula can be derived in (2.56). The coefficient of each order in (2.56), $c_i[n]$ and $d_i[n]$ should be determined. The calculation procedure is presented in the next section.

Table 2.5 Unknown variables represented by power series and the corresponding equations

Type	Unknown variables	Corresponding equations		
		Power balance	V constrant	Reciprocal relation
PQ	v, w^*	(2.51)	–	(2.55)
PV	v, w^*, Q	(2.52)	(2.53)	(2.55)
PVQ	v, w^*	(2.51)	(2.53)	(2.55)
P	v, w^*, Q	(2.52)	–	(2.55)
SL	–	–	(2.53)	–

$$\sum_{n=0}^{\infty} c_i[n]s^n \sum_{n=0}^{\infty} d_i[n]s^n = c_i[0]s^0 \cdot d_i[0]s^0 + s^1 \sum_{k=0}^{1} c_i[1-k] \cdot d_i[k] + s^2 \sum_{k=0}^{2} c_i[2-k] \cdot d_i[k] + \cdots + s^n \sum_{k=0}^{n} c_i[n-k] \cdot d_i[k] + \cdots \tag{2.56}$$

The tap-able transformer is always used to maintain a voltage magnitude at a target node by regulating the winding ratio, whereas the phase-shifting transformer is used to control the active power flow in the parallel branches by regulating the voltage angle across the transformer. In the load flow calculations, the general branch model can be presented in Fig. 2.5. The formulation is expressed in (2.57), where the branch model includes the transmission lines and the transformers. y_s and b_c are the series admittance and the shunt susceptance, respectively. τ and θ_{shift} are the transformer tap-ratio and the phase-shifting angle, i.e. $\tau = 1$ and $\theta_{shift} = 0$ in the case of representing a transmission line. The matrix (2.57) is symmetrical if the phases-shifting transformers are absent. The phase-shifting angles can change the off-diagonal entries of the branch models which results in an asymmetrical admittance matrix in the load flow calculations.

Note that the general branch model shown in Fig. 2.5 is split into series and shunt parts, Y_{ik}^{tr} and Y_i^{sh} in the canonical embedding, respectively. Therefore, the general branch model (2.57) is the summation of (2.58) and (2.59).

$$Y_{br} = \begin{bmatrix} \left(y_s + j\frac{b_c}{2}\right)\frac{1}{\tau^2} & -y_s \frac{1}{\tau e^{-j\theta_{shift}}} \\ -y_s \frac{1}{\tau e^{j\theta_{shift}}} & y_s + j\frac{b_c}{2} \end{bmatrix} \tag{2.57}$$

$$Y^{tr} = \begin{bmatrix} y_s \frac{1}{\tau e^{-j\theta_{shift}}} & -y_s \frac{1}{\tau e^{-j\theta_{shift}}} \\ -y_s \frac{1}{\tau e^{j\theta_{shift}}} & y_s \frac{1}{\tau e^{j\theta_{shift}}} \end{bmatrix} \tag{2.58}$$

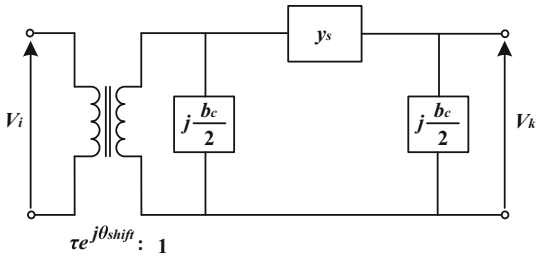


Fig. 2.5 The general branch model in load flow calculations [17]

$$Y^{sh} = \begin{bmatrix} \left(y_s + j\frac{b_c}{2}\right)\frac{1}{\tau^2} - \frac{y_s}{\tau e^{-j\theta_{shift}}} & 0 \\ 0 & \left(y_s + j\frac{b_c}{2}\right) - \frac{y_s}{\tau e^{j\theta_{shift}}} \end{bmatrix} \tag{2.59}$$

At the no-load condition, (2.60) can be obtained. In the no-load condition, i.e. $s = 0$, Eq. (2.60) is generally not valid if the phase-shifting angle is not 0 or the winding ratio is not 1, as the value of the diagonal element is not equal to the summation of the off-diagonal elements in (2.57). This is the reason to split the admittance matrix where the values of the diagonal elements of the matrix Y_{ik}^{tr} equal to the summation of the off-diagonal elements at each row as the shunt admittance Y^{sh} is separated from Y^{tr} and all current injections are zeros as $s = 0$ in the Eqs. (2.51), (2.52) and (2.54). This is the solution of the no-load condition. If assuming the slack voltage is $1\angle 0°$ at the no load condition, the voltages at all nodes will be $1\angle 0°$. Based on this assumption, the germ solution can ensure the converged solution being on the upper branch of the "nose" curve.

$$\sum_k Y_{ik}^{tr} v_k[0] = 0, \quad v_k[0] = 1 \tag{2.60}$$

After modifying the admittance matrix, the validity of the load flow Eqs. (2.51)–(2.55) and the calculation procedure are unchanged where only the admittance matrix is replaced by Y^{tr} and Y^{sh}. The original load flow equations are changed at the no-load condition due to the changes on the admittance matrix and the slack voltage. However, the load flow equations' recovery to the original load flow equations at $s = 1$, under which the expected solution is to be found.

2.3.5 HELM Calculation Procedure

The complete formulation of the embedded load flow equations are presented in (2.39) and (2.51)–(2.55) where the admittance matrices are modified to include tap-able and phase-shifting transformers. The power series can be applied to expand the unknown variables to the power series w.r.t. s.

A simple pattern can be demonstrated for PQ nodes [7].

$Y(v[0] + v[1]s^1 + v[2]s^2 + \cdots v[n]s^n) = (P + jQ)(w^*[0] + w^*[1]s^1 + w^*[2]s^2 + \cdots w^*[\mathrm{n}]s^n)s$	
To obtain $v[0]$	$s = 0$
$Y(v[0]) = 0 \rightarrow v[0]$ then $w^*[0] = f(v[0])$	
To obtain $v[1]$	Differentiating both sides w.r.t. s, and then substitute $s = 0$
$Y(v[1]) = (P + jQ)(w^*[0]) \rightarrow v[1]$ then $w^*[1] = f(v[1])$	
To obtain $v[2]$	Differentiating both sides w.r.t. s twice, and then substitute $s = 0$
$Y(v[2]) = (P + jQ)(w^*[1]) \rightarrow v[2]$ then $w^*[2] = f(v[2])$	

(continued)

(continued)

⋮	
To obtain $v[n]$	Differentiating both sides w.r.t. s n times, and then substitute $s = 0$
$Y(v[n]) = (P + jQ)(w^*[n-1]) \rightarrow v[\mathrm{n}]$ then $w^*[n] = f(v[n])$	
Solution	$v = v[0] + v[1] + v[2] + \ldots v[n]$

This pattern can be generalized for calculations of the power series coefficients at $s = 0$. It is carried out order by order, i.e. differentiating the power flow equations after power series expansions w.r.t s at both sides and evaluating at $s = 0$. The found coefficients of the power series order by order compose the germ solution which is used for Padé approximation to obtain the maximum convergence radius of the power series. The following content introduce the systematical way to implement HELM in the computer routine.

Step 1: $n = 0$

Calculate the coefficients at no-load condition by setting $s = 0$, then the power vanishes in the power flow equations, representing the no-load condition. Assuming the voltage at the slack node is $V_{sl}^{sp} = 1\angle 0°$, and then the voltage at all nodes are equal to V_{sl}^{sp}. It can be considered as a "flat start" shown in (2.61). It is a physical solution of the original load flow, i.e. it represents a condition that no power flows between any two nodes in the system. All calculations start from (2.61), which is also one of the reasons that HELM is independent of initial guess.

$$v_i[0] = 1 \; and \; Q_i[0] = 0 \tag{2.61}$$

Step 2: $n = 1$

Differentiating the load flow equation w.r.t s at both sides, evaluating at $s = 0$, and substituting the calculated coefficients from Step 1, obtain (2.62)–(2.69).

SL	$v_i[1] = V_{sl}^{sp} - 1$	(2.62)
PV	$\sum_k Y_{ik}^{tr} v_k[1] = P_i - Y_i^{sh}$	(2.63)
	$v_{i,re}[1] = \frac{V_i^{sp^2} - 1}{2}$	(2.64)
PQ	$\sum_k Y_{ik}^{tr} v_k[1] = (P_i - jQ_i) - Y_i^{sh}$	(2.65)
PVQ	$\sum_k Y_{ik}^{tr} v_k[1] = (P_i - jQ_i) - Y_i^{sh}$	(2.66)
	$v_{i,re}[1] = \frac{V_i^{sp^2} - 1}{2}$	(2.67)
P	$\sum_k Y_{ik}^{tr} v_k[1] = P_i - Y_i^{sh}$	(2.68)
All nodes	$W_i[1] = -W_i[0]$	(2.69)

Step 3: $n > 1$

The real and the imaginary parts of the voltage variables can be calculated separately, as the reactive power variables at PV and P nodes are embedded with s along the real axis. Continuously calculate finite numbers of orders using (2.70)–(2.77) until the active power mismatches at all nodes except for the slack node, and the reactive power mismatches at PQ and PVQ nodes are respectively within an acceptable band.

SL	$V_{slack}[n] = 0$	(2.70)
PV	$\sum_k Y_{ik}^{tr} v_k[n] = P_i \cdot w_i^*[n-1] - j\left(\sum_{k=1}^{n-1} Q_i[k] w_i^*[n-k]\right) - Y_i^{sh} v_i[n-1] - j\boldsymbol{Q_i}[\boldsymbol{n}]$	(2.71)
	$v_{i,re}[n] = -\frac{1}{2}\left(\sum_{k=1}^{n-1} v_i[k] v_i^*[n-k]\right)$	(2.72)
PQ	$\sum_k Y_{ik}^{tr} v_k[n] = (P_i - jQ_i) w_i^*[n-1] - Y_i^{sh} v_i[n-1]$	(2.73)
PVQ	$\sum_k Y_{ik}^{tr} v_i[n] = (P_i - jQ_i) w_i^*[n-1] - Y_i^{sh} v_i[n-1]$	(2.74)
	$v_{i,re}[n] = -\frac{1}{2}\left(\sum_{k=1}^{n-1} v_i[k] v_i^*[n-k]\right)$	(2.75)
P	$\sum_k Y_{ik}^{tr} v_k[n] = P_i \cdot w_i^*[n-1] - j\left(\sum_{k=1}^{n-1} K_i Q_\Sigma[k] w_i^*[n-k]\right) - Y_i^{sh} v_i[n-1] - j\boldsymbol{K_i Q_\Sigma}[\boldsymbol{n}]$	(2.76)
All nodes except for SL	$w_i[n] = -\sum_{k=0}^{n-1} \frac{w_i[k] \cdot v_i[n-k]}{v_i[0]}$	(2.77)

The real part of the voltage variables at PV and PVQ nodes in (2.64) and (2.67) at $n = 1$, and (2.72) and (2.75) when $n > 1$, are derived in (2.78) by (i) applying (2.56) to (2.53) and equating the coefficients for each order of s; (ii) starting from (2.61).

$$\begin{aligned}
v_i[0] \cdot v_i[0]^* &= 1 \rightarrow v_i[0]^* = 1 \\
v_i[0] \cdot v_i[1]^* + v_i[1] \cdot v_i[0]^* &= V_i^{sp^2} - 1 \rightarrow v_{i,re}[1] = \frac{V_i^{sp^2} - 1}{2} \\
v_i[0] \cdot v_i[2]^* + v_i[1] \cdot v_i[1]^* + v_i[2] \cdot v_i[0]^* &= 0 \rightarrow v_{i,re}[2] = -\frac{1}{2} v_i[1] \cdot v_i[1]^* \\
v_i[0] \cdot v_i[3]^* + v_i[1] \cdot v_i[2]^* + v_i[2] \cdot v_i[1]^* + v_i[3] \cdot v_i[0]^* &= 0 \rightarrow v_{i,re}[3] \\
&= -\frac{1}{2}(v_i[1] \cdot v_i[2]^* + v_i[2] \cdot v_i[1]^*) \\
&\vdots \\
V_{i,re}[n] &= -\frac{1}{2}\left(\sum_{k=1}^{n-1} V_i[k] V_i^*[n-k]\right)
\end{aligned} \tag{2.78}$$

If splitting the admittance matrix and the voltage into real and imaginary parts as shown in (2.79), then (2.71)–(2.76) can be represented in (2.80) where the unknown reactive power injections at PV and PVQ nodes are moved to the left hand sides of

equations, whereas the known voltage real parts at PV and PVQ nodes are moved to the right hand sides.

$$\sum Y^{tr} v = \sum \left((G v_{re} - B v_{im}) + j(B v_{re} + G v_{im}) \right) \tag{2.79}$$

$$\begin{pmatrix} V[n] \\ Q[n] \end{pmatrix} = f\left(\sum_{V[k]}^{n-1} V[k], \sum_{k=0}^{n-1} Q[k] \right) \tag{2.80}$$

Equation (2.81) is a recursive step of (2.80) for $n > 1$, where the coefficients of s^n are found based on the coefficients of s^0 to s^{n-1} orders that are shown in (2.83)–(2.86).

In (2.81), $PQ[n-1]$ and $PVQ[n-1]$ are the right hand sides of (2.73) and (2.74), respectively. $PV[n-1]$ and $P[n-1]$ are the right hand sides of (2.71) and (2.76), respectively, after moving the unknown $Q_{pv}[n]$ and $Q_p[n]$ to the left hand side of (2.81).

From Step 3, the voltage at the slack node is absent from calculations. Each entry in (2.81) represents a matrix or a vector where $Q_\Sigma[n]$ represents the total required reactive power at corresponding PVQ node to maintain the voltage magnitude which is placed in the corresponding PVQ rows in (2.81). $K_{p,pvq}$ is the participation factor matrix for all coupled P/PVQ pairs which is presented in form of (2.82). $I_{pv,pv}$ is an identity matrix. In the recursive calculation, the individual reactive power injection at each P node,$Q_{p1\ldots N}$, is obtained via (2.8) and found $Q_\Sigma[n] \in \mathcal{R}^{(N_{pvq} \times 1)}$ in each order.

$$\begin{bmatrix}
I_{ref,ref} & 0 & 0 & 0 & 0 & 0 & 0 & 0 & 0 & 0 \\
0 & I_{ref,ref} & 0 & 0 & 0 & 0 & 0 & 0 & 0 & 0 \\
G_{pq,ref} & -B_{pq,ref} & G_{pq,pq} & -B_{pq,pq} & -B_{pq,pv} & 0 & -B_{pq,pvq} & 0 & G_{pq,p} & -B_{pq,p} \\
B_{pq,ref} & G_{pq,ref} & B_{pq,pq} & G_{pq,pq} & G_{pq,pv} & 0 & G_{pq,pvq} & 0 & B_{pq,p} & G_{pq,p} \\
B_{pv,ref} & G_{pv,ref} & B_{pv,pq} & G_{pv,pq} & G_{pv,pv} & I_{pv,pv} & G_{pv,pvq} & 0 & B_{pv,p} & G_{pv,p} \\
G_{pv,ref} & -B_{pv,ref} & G_{pv,pq} & -B_{pv,pq} & -B_{pv,pv} & 0 & -B_{pv,pvq} & 0 & G_{pv,p} & -B_{pv,p} \\
B_{pvq,ref} & G_{pvq,ref} & B_{pvq,pq} & G_{pvq,pq} & G_{pvq,pv} & 0 & G_{pvq,pvq} & 0 & B_{pvq,p} & G_{pvq,p} \\
G_{pvq,ref} & -B_{pvq,ref} & G_{pvq,pq} & -B_{pvq,pq} & -B_{pvq,pv} & 0 & -B_{pvq,pvq} & 0 & G_{pvq,p} & -B_{pvq,p} \\
G_{p,ref} & -B_{p,ref} & G_{pvq,pq} & -B_{p,pq} & -B_{p,pv} & 0 & -B_{p,pvq} & 0 & G_{p,p} & -B_{p,p} \\
-B_{p,ref} & G_{p,ref} & B_{p,pq} & G_{p,pq} & G_{p,pv} & 0 & G_{p,pvq} & \boldsymbol{K_{p,pvq}} & B_{p,p} & G_{p,p}
\end{bmatrix} \cdot \begin{bmatrix}
V_{sl,re}[n] \\ V_{sl,im}[n] \\ v_{pq,re}[n] \\ v_{pq,im}[n] \\ v_{pv,im}[n] \\ \boldsymbol{Q_{pv}[n]} \\ v_{pvq,im}[n] \\ \boldsymbol{Q_\Sigma[n]} \\ v_{p,re}[n] \\ v_{p,im}[n]
\end{bmatrix}$$

$$= \begin{bmatrix}
V_{sl}^{sp} - 1, \text{ if } n = 1 \text{ and } 0, \text{ if } n > 1 \\ 0 \\ Real(PQ[n-1]) \\ Imag(PQ[n-1]) \\ Imag(PV[n-1]) \\ Real(PV[n-1]) \\ Imag(PVQ[n-1]) \\ Real(PVQ[n-1]) \\ Real(P[n-1]) \\ Imag(P[n-1])
\end{bmatrix} - \begin{bmatrix} 0 \\ 0 \\ G_{pq,pv} \\ B_{pq,pv} \\ B_{pv,pv} \\ G_{pv,pv} \\ B_{pvq,pv} \\ G_{pvq,pv} \\ G_{p,pv} \\ B_{p,pv} \end{bmatrix} \cdot v_{pv,re}[n] - \begin{bmatrix} 0 \\ 0 \\ G_{pq,pvq} \\ B_{pq,pvq} \\ B_{pv,pvq} \\ G_{pv,pvq} \\ B_{pvq,pvq} \\ G_{pvq,pvq} \\ G_{p,pvq} \\ B_{p,pvq} \end{bmatrix} \cdot v_{pvq,re}[n] \tag{2.81}$$

$$K_{p,pvq} = \begin{bmatrix} K_{p_1,pvq_1} & & & \\ \vdots & 0 & \cdots & 0 \\ K_{p_n,pvq_1} & & & \\ & K_{p_2,pvq_2} & & \\ 0 & \vdots & \cdots & 0 \\ & K_{p_n,pvq_2} & & \\ \vdots & \vdots & \ddots & \vdots \\ & & & K_{p_1,pvq_n} \\ 0 & 0 & \cdots & \vdots \\ & & & K_{p_n,pvq_n} \end{bmatrix}^{N_p \times N_{pvq}} \tag{2.82}$$

$$PQ[n-1] = \left(s_{pq} \cdot w_{pq}[n-1]\right)^* - Y_{pq}^{sh} v_{pq}[n-1] \tag{2.83}$$

$$PV[n-1] = Real\left(s_{pv}\right) \cdot w_{pv}^*[n-1] - j\left(\sum_{k=1}^{n-1} Q_{pv}[k] w_{pv}^*[n-k]\right) - Y_{pv}^{sh} v_{pv}[n-1] \tag{2.84}$$

$$PVQ[n-1] = \left(s_{pvq} \cdot w_{pvq}[n-1]\right)^* - Y_{pvq}^{sh} v_{pvq}[n-1] \tag{2.85}$$

$$P[n-1] = Real\left(s_p\right) \cdot w_p^*[n-1] - j\left(\sum_{k=1}^{n-1} K_{p,pvq} Q_\Sigma[k] w_p^*[n-k]\right) - Y_p^{sh} v_p[n-1] \tag{2.86}$$

Step 4: Obtain the values of the power series

As long as coefficients of a new order of the power series are obtained, the variables' values can be found by summation of their power series. However, as mentioned, this approach is limited by the radius of convergence of the power series. Therefore, the analytical continuation is applied to obtain the maximum convergence radius of the power series. As long as a new order of power series is solved by (2.81), the analytical continuation should perform to update the voltage values. The recursive calculation stops if the active power mismatches at PQ, PV, PVQ and P nodes and the reactive power mismatches at PQ and PVQ nodes are within an acceptable band. Other types of control functions can also be embedded to HELM, for example, the voltage magnitude controlled by the transformer tap ratio shown in Appendix A—Voltage control by tap ratio in HELM.

As shown in Table 2.6, the calculation is straightforward through (2.81) where the left-hand-side is constructed only once, and the right hand side needs some loops for the convolution calculations for (2.84) and (2.86). The most time consuming task is Padé approximation, i.e. line 10 in Table 2.6. However, the Padé approximation is carried out independently for each node which can be calculated in parallel. Moreover, the matrix (2.36) for each node can be stored and reused if

Table 2.6 The load flow algorithm applying HELM

1	*Calculate ΔP for PV, PQ, PVQ and P nodes, and ΔQ for PQ and PVQ nodes;*
2	*if $\|\Delta P\|_n \geq \varepsilon$ or $\|\Delta Q\|_n \geq \varepsilon$*
3	*Construct the left-hand-side of (2.81)*
4	*Construct the right-hand-side of (2.81) for n = 1, (2.62)-(2.69)*
5	*Calculate unknown variable for n=1.*
6	*while $n \leq N_{max}$*
7	*Construct the right-hand-side of (2.81) for n > 1, (2.83)-(2.86)*
8	*Calculate coefficients of the power series for the unknown variables at n^{th} order*
9	*if $n \geq 3$*
10	*Construct the matrix (2.36) of Padé approximation for each node, v_i*
11	*Find the value of power series for each node via three-terms recursive formula (2.37)*
12	*Calculate ΔP for PV, PQ, PVQ and P nodes, and ΔQ for PQ and PVQ nodes;*
13	*if $\|\Delta P\|_n < \varepsilon$ and $\|\Delta Q\|_n < \varepsilon$*
14	*break;*
15	*end*
16	*end*
17	*end*
18	*end*

there is sufficient RAM [7], i.e. the matrix will be extended only when there is a new order available. In this way, the calculation time is foreseen to be able to be greatly reduced.

2.3.6 Case Studies with HELM

The same example shown in Fig. 2.3 is used to demonstrate HELM calculations, where the active power consumption at Bus 25 is increased from 224 MW until the load flow calculation fails to be converged. The voltage collapses when the load at Bus 25 increases beyond 2500 MW. A new case is created every instant where the load at Bus 25 is stepwise increased by 100 MW. In different load levels at Bus 25, the voltage magnitudes at PVQ nodes, i.e. Bus 11 and Bus 22, are kept constant due to the generator remote voltage control.

The reactive power outputs from Gen 31, Gen 32, Gen 35 and Gen 36 at P nodes are shown in Fig. 2.6. In order to keep the voltage at P nodes, i.e. Bus 11 and Bus 22 in Fig. 2.3, the reactive power outputs at Gen 31, Gen 32, Gen 35 and Gen 36 are needed to be respectively increased where their contributions are according to the predefined participation factors that are constants for different simulated cases. As shown in the dash lines in Fig. 2.6, though the reactive power output of each generator increases along simulation cases, the ratios of the participation factor are unchanged. The calculations stops at the breaking case, i.e. Case 25 where no result is presented in Fig. 2.6.

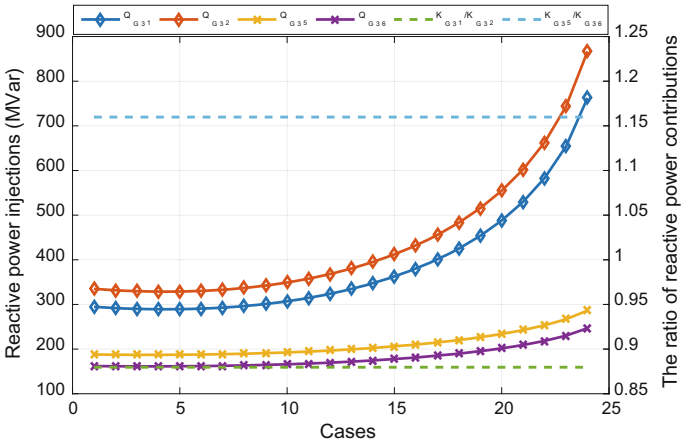


Fig. 2.6 The reactive power at P nodes to control the voltage at corresponding PVQ nodes corresponding to the constant participation factors

In all cases, Padé approximation is carried out sequentially node by node and the matrix (2.36) is reconstructed once a new order is available. In these studies, the generator reactive power limits are not considered in the calculations, which can be implemented in the outer loop, changing the PV to PQ nodes once the reactive power limit is reached.

The studies are carried out at a PC with Intel® Core i7-4600 M dual 2.90 GHz CPU and 16 GM RAM. As shown in Fig. 2.7, compared to the NR method, the time consumption of the simulated cases for HELM are generally longer. In these cases, HELM needs to reconstruct the matrices (2.36) for the power series in the continued faction calculations that significantly increases the time consumption. However, HELM with continued faction approach is independent of initial guesses and guarantees the convergence if the solution is physically existing which is superior to the approach based on NR method. For example, if the initial voltage magnitudes at Bus 24 and Bus 28 are changed, the approach based on NR method fails to be converged in many cases as shown in Fig. 2.8, where each pixel in the map represents a load flow calculation with different initial guesses of the voltage magnitudes at Bus 24 and Bus 28. Moreover, many results are in fact the infeasible solutions, which locate at the lower branches of the "nose" curves. In contrast, HELM provides the solutions with the same time consumptions no matter what the initial values are, as HELM starts from the no-load condition without any initial guess.

The system condition is changed, i.e. the active power and the reactive power consumptions at Bus 25 are changed to 100 MW and 500 MVar, respectively. Different voltage magnitude at PVQ nodes, Bus 11 and Bus 22, are varied from 0.6

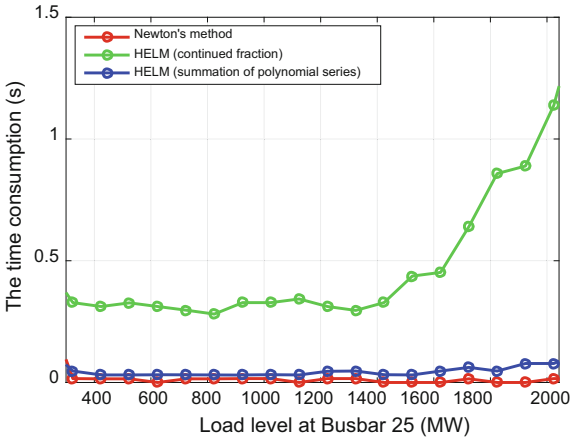


Fig. 2.7 Comparisons of the time consumptions for (i) summation of the power series; (ii) continued fraction and (iii) Newton-Raphson method

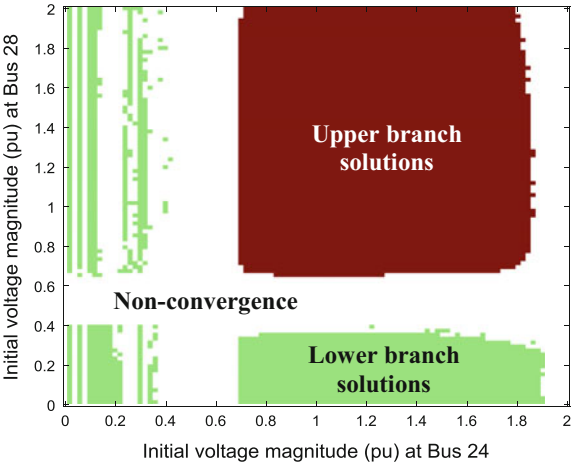


Fig. 2.8 The convergence map of different initial points for total 101 × 101 load flow calculations based on the Newton-Raphson method in the test grid. The initial voltage magnitudes at Bus 24 and Bus 28 are varied from 0 to 2 pu with 0.02 pu. interval. Red: upper-branch solutions; Green: lower-branch solutions

pu to 1.6 pu, respectively. The voltage set points at Bus 11 and Bus 22 are in some cases unrealistic. However, these cases are only used to compare the convergence ability of HELM with the continued fraction to the NR method with the flat start.

The convergence maps of the NR method with the flat start and HELM with the continued fraction are presented in Figs. 2.9 and 2.10, respectively, where both the maximum iteration number of the NR method and the maximum order of the power series in HELM are set to 50. More cases are converged based on HELM than NR method. Moreover, the solutions based on HELM are guaranteed to be feasible, whereas the solutions based on NR method may be unstable equilibrium points.

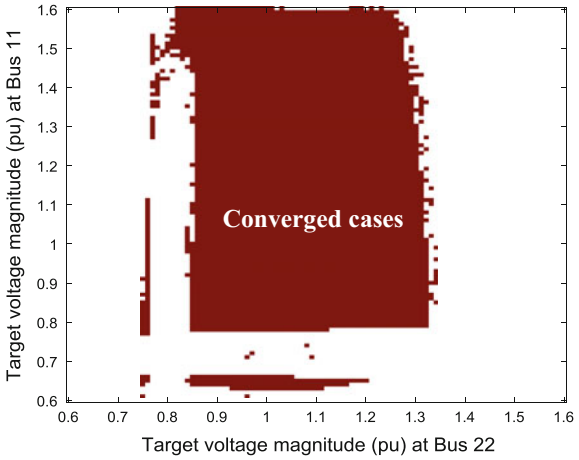


Fig. 2.9 The convergence map of the NR method in the test grid with different voltage magnitudes at PVQ nodes, i.e. Bus 11 and Bus 22, respectively. The target voltage magnitudes at Bus 11 and Bus 22 are varied from 0.6 pu to 1.6 pu with 0.01 pu. interval. Red: the converged cases without identifying the upper or lower branch solutions

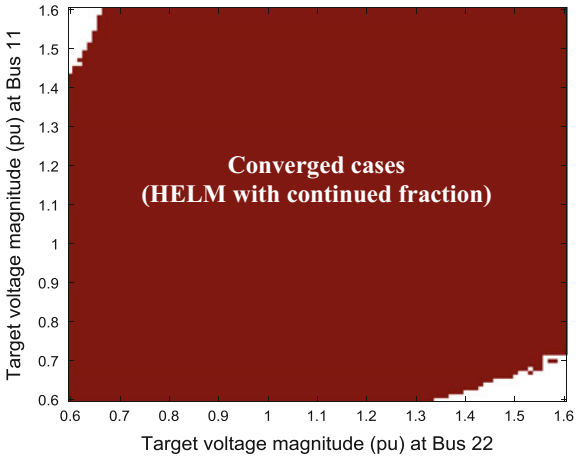


Fig. 2.10 The convergence map of HELM in the test grid with different voltage magnitudes at PVQ nodes, i.e. Bus 11 and Bus 22, respectively. The target voltage magnitudes at Bus 11 and Bus 22 are varied from 0.6 pu to 1.6 pu with 0.01 pu. interval. Red: the converged cases

2.4 Summary

The load flow equations are nonlinear, which can be solved via the NR method. An alternative method is HELM which applies the complex analysis to solve load flow equations. In the real-time system, the system load flow condition is obtained via the State Estimator (SE) where redundant inputs are available from the measurement devices. The purpose is to project the measurement data into a predefined network model where the errors are minimized. The objective of SE is thus to formulate the load flow problem into an optimization framework and then minimize the total error via least-square concept. In this framework, NR is better than HELM as the optimization requires the Jacobian matrix to determine the searching direction for achieving the objective while complying with all constraints. In contrast,

HELM is not able to provide the information for searching direction. However, it is an alternative and useful tool for the load flow calculation, especially in the abnormal condition where NR is difficult to converge.

HELM can be applied as an identification tool to verify if a load flow condition is physically existing after the AVC find a solution. It can provide a reliable solution for the real-time voltage control system. In addition, it can be potentially applied for diagnosis of the abnormal load flow conditions. Moreover, the future work of utilization HELM in the AVC system will be to develop a promising optimization algorithm that can compete with the existing Newton iteration-based optimization framework for the decision making process.

References

1. Popovic DS, Levi VA (1992) Extension of the load flow model with remote voltage control by generator. Electr Power Syst Res 25(3):207–212
2. Tinney W, Hart CE (1967) Power flow solution by newton's method. IEEE Trans Power Apparatus Syst PAS-86(11):1449–1460
3. Iwamoto S, Tamura Y (1978) A fast load flow method retaining nonlinearity. IEEE Trans Power Apparatus Syst PAS-97(5):1586–1599
4. Iwamoto S, Tamura Y (1981) A load flow calculation method for Ill-conditioned power systems. IEEE Trans Power Apparatus Syst PAS-100(4):1736–1743
5. Schaffer MD, Tylavsky DJ (1988) A nondiverging polar-form Newton-based power flow. IEEE Trans Ind Appl 24(5):870–877
6. Ajjarapu V, Christy C (1992) The continuation power flow: a tool for steady state voltage stability analysis. IEEE Trans Power Syst 7(1):416–423
7. Trias A (2012) The holomorphic embedding load flow method. IEEE PES GM, San Diego
8. Baghsorkhi SS, Suetin SP (2015) Embedding AC power flow with voltage control in the complex plane: the case of analytic continuation via padé approximants, arXiv.org. Available online http://arxiv.org/pdf/1504.03249v1.pdf
9. Trias A (2015) Fundamentals of the holomorphic embedding load-flow method, arXiv.org. http://arxiv.org/pdf/1509.02421.pdf, Sep. 2015
10. Subramanian MK (2014) Application of holomorphic embedding to the power-flow problem. Master Thesis, Arizona State University
11. Subramanian MK, Feng Y, Tylavsky D (2013) PV bus modeling in a holomorphically embedded power-flow formulation. North American Power Symposium, Manhattan
12. Baker G, Graves-Morris P (1996) Padé approximants, series: encyclopaedia of mathematics and its applications. Cambridge University Press, New York
13. Stahl H (1989) On the convergence of generalized padé approximants. Constr Approximation 5(1):221–240
14. Stahl H (1997) The convergence of padé approximants to functions with branch points. J Approximation Theory 91(2):139–204
15. Cuyt A, Wuytack L (1987) Nonlinear methods in numerical analysis. North Holland
16. Cuyt A, Petersen VB, Verdonk B, Waadeland H, Jones WB (2008) Handbook of continued fractions for special functions. Springer, Berlin
17. Zimmerman RD, Murillo-Sanchez CE, Thomas RJ (2011) MATPOWER: steady-state operations, planning, and analysis tools for power systems research and education. IEEE Trans Power Syst 26(1):12–19

http://www.springer.com/978-3-319-69885-4

Voltage Control in the Future Power Transmission Systems

Qin, N.

2018, XXIV, 240 p. 119 illus., 104 illus. in color.,
Hardcover
ISBN: 978-3-319-69885-4